

Micromachined antenna-coupled uncooled microbolometers for terahertz imaging arrays

A. J. Miller, A. Luukanen, E. N. Grossman

Quantum Electrical Metrology Division, National Institute of Standards and Technology*
325 Broadway, Boulder, CO USA 80305

ABSTRACT

In recent years our group has made significant progress toward the goal of a scalable, inexpensive terahertz imaging system for the detection of weapons concealed under clothing. By actively illuminating the subject under examination with only moderate source power (few milliwatts) the sensitivity constraints on the detector technology are significantly lessened compared to purely passive millimeter-wave detection. Last year, we demonstrated a fully planar, optically lithographed, uncooled terahertz imaging array with 120 pixels on a silicon substrate 75 mm in diameter. In this paper we present the recent progress on improving the responsivity of the individual microbolometers by a simple technique of surface micromachining to reduce the substrate thermal conduction. We describe the microbolometer array fabrication and present results on devices with a measured electrical responsivity of over 85 V/W (electrical NEP ≈ 25 pW/ $\sqrt{\text{Hz}}$), an improvement by a factor of two over current substrate-supported bolometers.

Keywords: air-bridge, microbolometer, millimeter-wave, planar antenna, terahertz imaging

1. INTRODUCTION

As reported previously¹⁻⁴ and elsewhere in this conference,^{5,6} using room-temperature metallic (Nb) bolometers with integrated planar lithographic antennas (currently Al, or Au in previous designs), we have built and tested an active 120-element video-rate staring focal-plane array (FPA) operating at 95 GHz. Besides the obvious work toward increasing the number of pixels in the acquired image, we are also improving the performance of the individual pixels to enable higher signal-to-noise images and longer-range signal detection. Furthermore, improved pixel sensitivity is highly desired to reduce the source power requirements when considering the operation of bolometers at higher frequency (e.g., >500 GHz) where a low-sensitivity active imaging system would require increasingly complex and expensive sources.

In this paper we describe simple fabrication steps that are used to improve the responsivity of our FPA pixels by a factor of almost two over existing substrate-supported pixel designs. To achieve these improvements we use a straightforward method of surface micromachining to release the metallic bolometers from the substrate, thereby reducing the thermal conduction to the substrate and improving the measured signal for a given incident optical power.

2. DETECTOR BASICS

Each pixel of the millimeter-wave FPA is a planar slot-ring design antenna tuned for operation at 95 GHz coupled to a purely resistive bolometer.³ The bolometer resistance ($\sim 200 \Omega$) is designed for efficient coupling of power from the antenna into the bolometer. The incoming millimeter-wave power is converted into heat in the current-biased bolometer and the corresponding change in resistance is measured by monitoring the voltage drop across the bolometer.

* Contribution of the U.S. Government; not subject to copyright.
E-mail: ajmiller@boulder.nist.gov, Telephone: (303) 497-4212

The voltage across the bolometer in the absence of optical power is given by $v = iR = i(R_0 + \Delta R)$, where i is the current bias of the device, R_0 is the zero-bias device resistance and ΔR is the change in resistance of the bolometer due to bias-induced temperature changes. Classical metallic bolometers such as ours have a positive temperature coefficient of resistance resulting in $\Delta R > 0$ under a constant current bias. This resistance change can be written as $\Delta R = \beta iv$, where $\beta = G^{-1}dR/dT$. For a fixed dR/dT , the total thermal conduction to the surrounding environment (heat bath), G , determines the ultimate sensitivity of the bolometer. The lower the G the higher the temperature rise of the bolometer for a given input power and, therefore, a larger resistance and resulting voltage signal.

On the other hand, a low G will also slow down the bolometer response. For our active system we desire the lowest G possible while maintaining a bolometer time constant below $\sim 10 \mu\text{s}$ to enable the next-generation of scanned imaging system.⁶ Our current generation of bolometers has a time constant much smaller than required ($\tau_{\text{bolo}} \approx 400 \text{ ns}$). As a result, we have margin to decrease G , slow down the device, and improve device sensitivity by a factor of 20 without sacrificing any design goals of the scanned active system.

The total thermal conduction from the bolometer to the heat bath is a sum of the electronic component of the thermal conduction intrinsic to the bolometer itself, G_{elec} , and the phonon component of the conduction of the bolometer plus the substrate, G_{phon} . In the substrate-supported bolometer design, G is determined by the thickness of the oxide layer underneath the bolometer and is made as thick as possible to minimize G . In our air-bridge design we attempt to eliminate this contribution to the G by etching the substrate out from under the bolometer.

It should be noted that also inherent in our design choice is the self-imposed limitation of requiring our array fabrication process to remain as simple as possible to ensure that production costs for a commercial system are reasonably low. The process described in the following section meets all of these requirements, i.e., improving pixel response, increasing the bolometer thermal relaxation time, and maintaining a viable commercial process.

3. DEVICE FABRICATION

An overview of the fabrication of both the substrate-supported and air-bridge microbolometer FPAs is shown in Fig. 1. We begin with high-resistivity Si wafers ($\rho > 5,000 \Omega\text{-cm}$) to ensure low loss at 100 GHz. The wafers are oxidized using a standard wet oxidation to grow either a thin oxide ($\sim 50 \text{ nm}$) for the air-bridge process, or a thick oxide ($\sim 1.8 \mu\text{m}$) for the substrate-supported process. Next, the bolometer metal ($\sim 35 \text{ nm Nb}$) is deposited with dc magnetron sputtering followed by the antenna metal ($\sim 220 \text{ nm Al}$). These metals are deposited as a bilayer without breaking vacuum between depositions. The antenna layer is patterned using the antenna-layer mask (Fig. 1a) and standard projection lithography. The metal is etched using a wet Al etch (Transene Type A) that has excellent selectivity to Nb.

Next, the bolometer is patterned using the bolometer mask (Fig. 1b) and etched using an SF_6 dry reactive-ion etch (RIE). This etch is followed by the deposition of the crossover wiring insulation layer (250 nm PECVD SiO_2 , Fig. 1c). The wiring vias are etched using an RIE process with a recipe to give 45-degree sloped sidewalls to ensure good step-coverage of the final wiring layer. The wiring layer (300 nm Al) is deposited, patterned, and wet-etched leaving a cross-section as shown in Fig. 1d. This figure shows the bolometer covered by SiO_2 , as is the case for the air-bridge devices, as described below; however, we have the option of reducing the thermal conduction further by etching the insulator off the Nb during the via etch. This is done routinely and was the process used to fabricate, for instance, the FPAs in Refs. 6 and 1. For the substrate-supported bolometer process the final step is a deep-RIE (Bosch process) thinning of the wafer to ensure that it is thin enough to emulate a free-space antenna³ ($< 50 \mu\text{m}$ thick).

The air-bridge process includes one additional step. Before the deep-RIE backside etch, a final mask and RIE oxide etch are used to remove the insulator oxide and the (thin) substrate oxide next to the bolometer on both sides. The backside deep-RIE step is performed and the wafer is cleaned of all photoresist and then placed

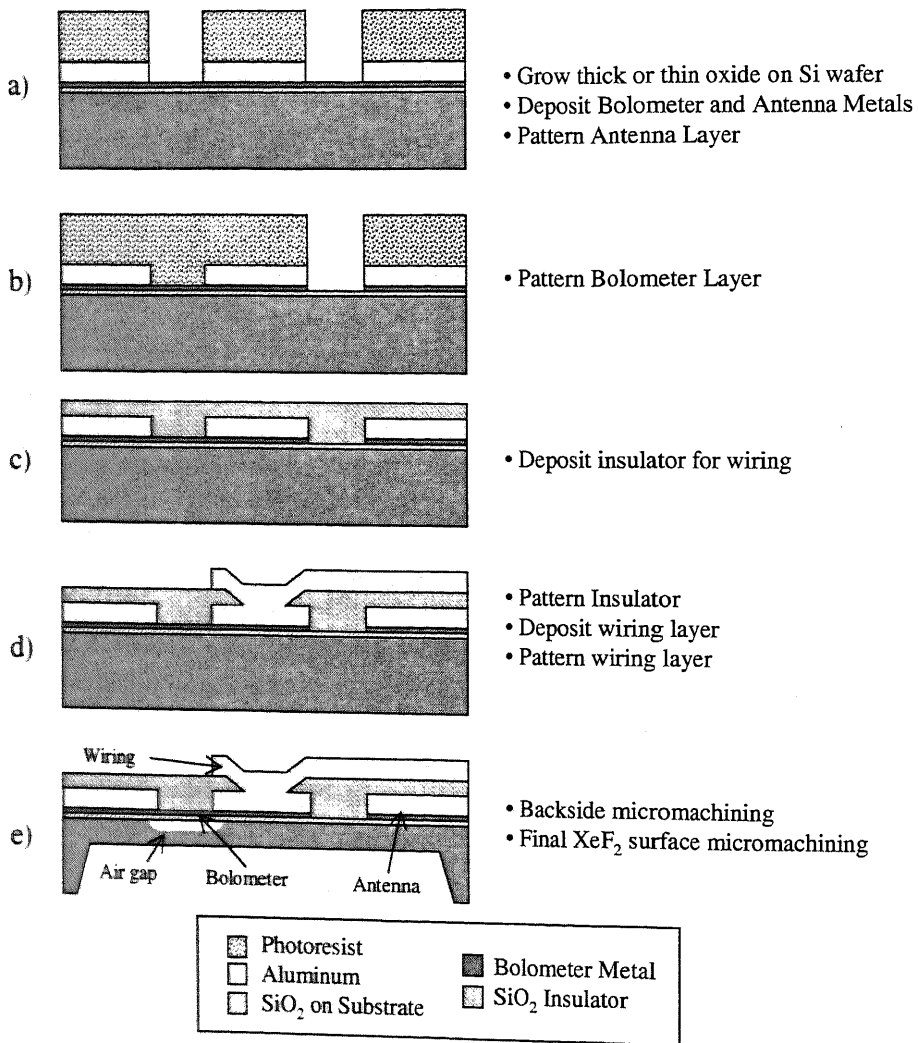


Figure 1. Diagram of the complete device fabrication process including the antenna and bolometer definition and final substrate removal steps.

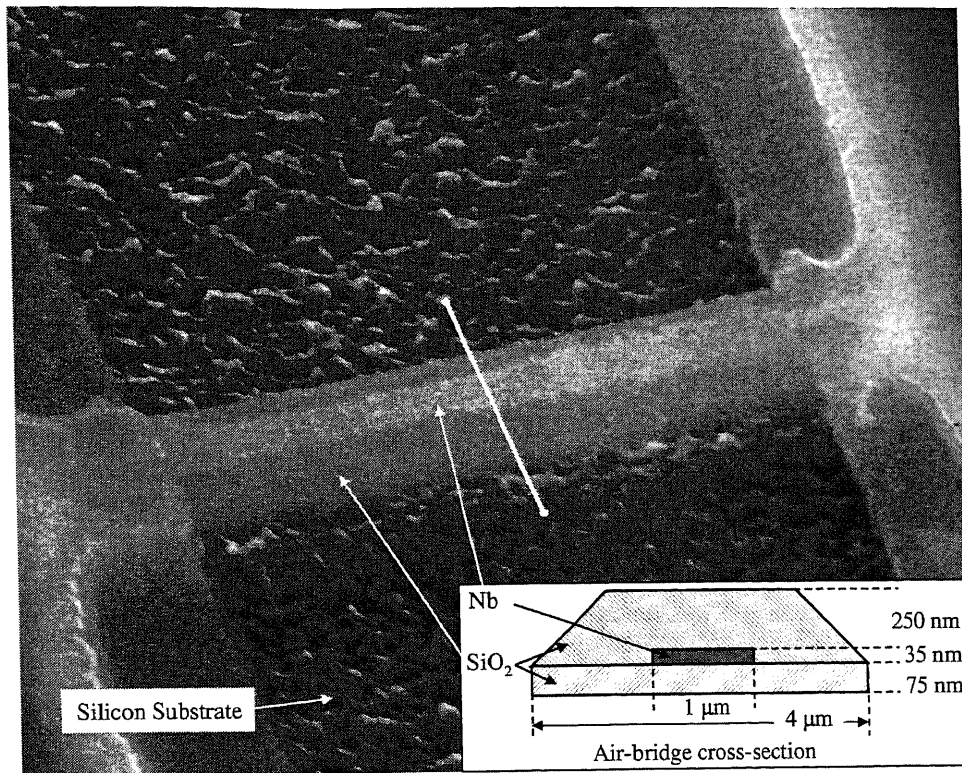


Figure 2. Scanning electron micrograph of a finished SiO_2 -encapsulated Nb microbolometer. The figure inset shows a schematic of the cross-section of the bolometer and the encapsulating oxide.

into a XeF_2 gas-phase chemical etching system. XeF_2 isotropically etches the Si substrate out from underneath the bolometer, leaving a free-standing, oxide-encapsulated air-bridge. An SEM photo of one such bolometer is shown in Fig. 2 along with an inset showing the cross-sectional dimensions of the air-bridge. The air-bridge is nominally $10 \mu\text{m}$ long, $4 \mu\text{m}$ wide, and $<500 \text{ nm}$ thick. The Nb bolometer is $10 \mu\text{m}$ long, $1 \mu\text{m}$ wide, and $\sim 35 \text{ nm}$ thick. The airgap distance is between $2 \mu\text{m}$ and $5 \mu\text{m}$ from the underlying Si substrate.

4. RESULTS

The devices were tested using a simple setup that allows a dc current bias while monitoring the dc voltage drop across the device. In addition, a small ac bias was applied at a frequency of 1 kHz , and the ac voltage was monitored with a lock-in amplifier. In this way both the dc i - v curve and the differential resistance (dv/di) were measured simultaneously. Furthermore, the device is mounted in a small vacuum chamber on a stage whose temperature is regulated using a closed-loop thermoelectric cooler and thermocouple. This measurement setup enables detailed dv/di vs. temperature curves to be compiled. A typical set of data are shown in Fig. 3. Note that the lowest-temperature curves are spaced by 5 degrees, and the highest are spaced by 10 degrees.

Of particular note is the decrease in differential resistance of the device as the bias is increased and the resulting (apparent) negative TCR at low bias. This behavior is seen on all of the devices fabricated so far using the Al/Nb process described in Sec. 3 and is consistent with a current-dependent resistance in series with the bolometer that is thermally inactive. This is confirmed by the fact that the zero-bias resistance as a function of temperature shows only positive TCR effects ($\text{TCR} = 0.15 \text{ \%}/\text{K}$). This is seen in Fig. 3 as a monotonic increase in R_0 as the substrate temperature is increased. It is unclear where this anomalous resistance originates. It

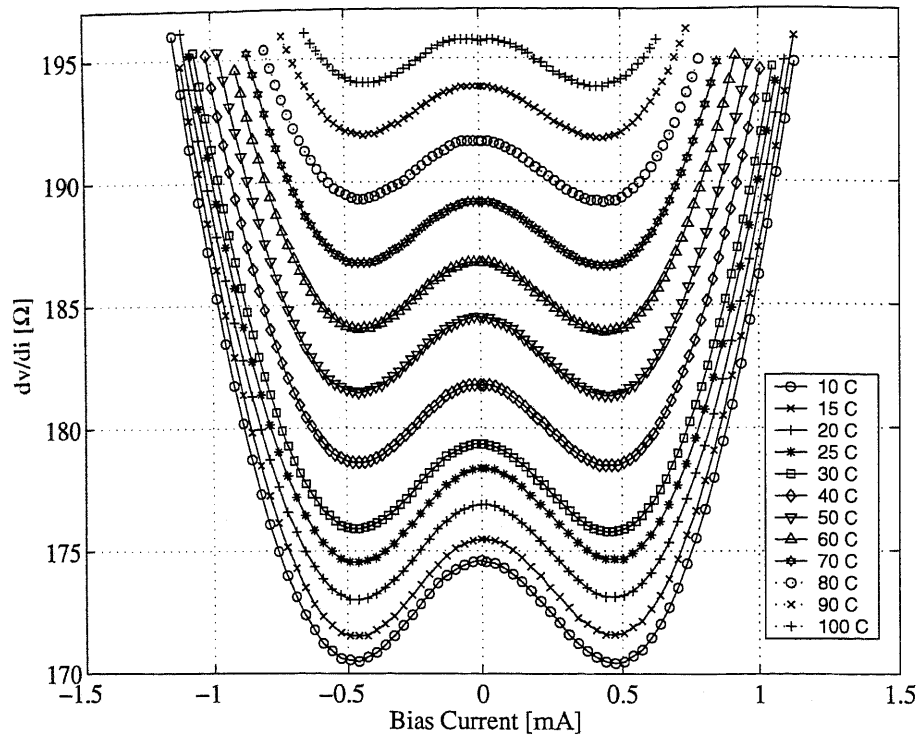


Figure 3. Differential resistance (dv/di) as a function of temperature for an SiO_2 -encapsulated Nb air-bridge microbolometer.

is unlikely to be caused at the wiring-to-antenna Al-Al interface because on-chip test structures designed to measure such interfaces show no abnormal behavior. Additionally, it is unlikely to be from an unclean Al-Nb interface because these metals are deposited *in situ*. We are currently investigating this effect and expect to eliminate it in future devices. Fortunately, the bolometers are able to be biased at currents high enough to make the contribution from this anomalous resistance negligible.

Neglecting the anomaly at low bias, the expected form of the dv/di vs. i curve can be derived as follows. From Sec. 2, $v = iR = i(R_0 + \beta iv)$. Solving for v and differentiating with respect to i gives

$$\frac{dv}{di} = \frac{R_0(1 + i^2\beta)}{(1 - i^2\beta)^2} \quad (1)$$

and because $\beta = G^{-1}dR/dT$ we can extract the thermal conduction from β .

Fig. 4 shows dv/di for the same air-bridge microbolometer in an evacuated environment compared to an ambient air environment. Also shown are two plots of eq. 1 with $\beta = 36.5 \text{ V}/(\text{W}\cdot\text{mA})$ and $\beta = 53.7 \text{ V}/(\text{W}\cdot\text{mA})$ and $R_0 = 161.3 \Omega$ fixed by higher-current measurements of the same bolometer. These values of β were picked manually to give good visual agreement at high currents because a fit would have required using just the uppermost few data points to avoid the low-current resistance anomaly. Later measurements to higher currents show irreversible changes (burnout) of the bolometer at a current of 1.7 mA. Therefore the maximum responsivity of this device was measured at $85.9 \text{ V}/\text{W}$ (electrical $\text{NEP} \approx 25 \text{ pW}/\sqrt{\text{Hz}}$) biased at 1.6 mA. This is an improvement by a factor of five over much of our previous work¹⁻³ and a factor of two better than our best substrate-supported devices to date.⁵

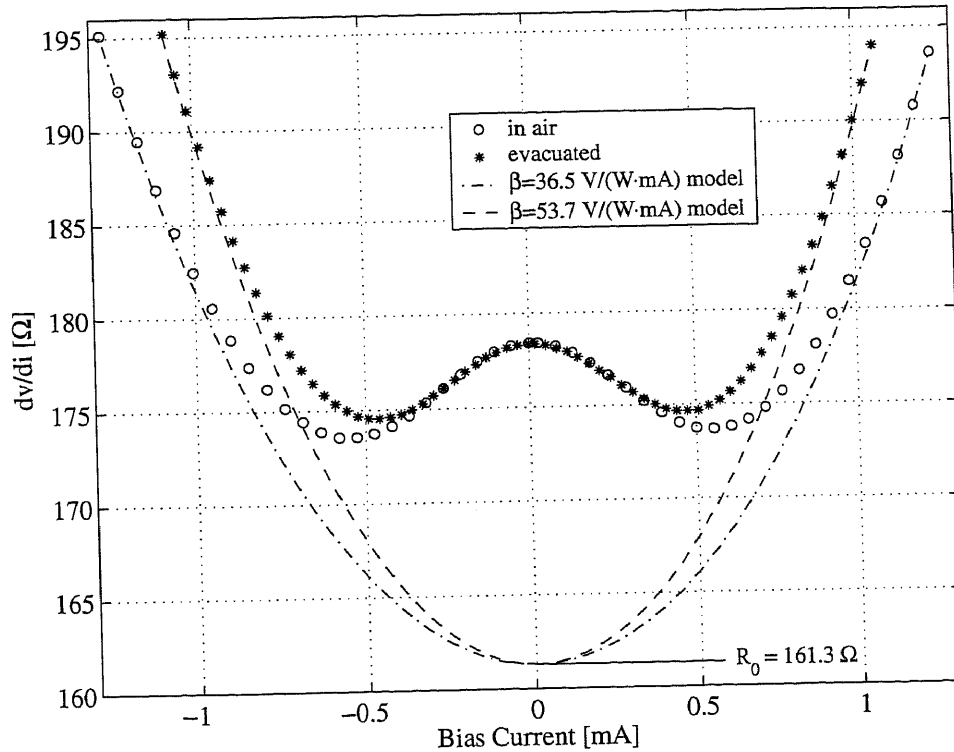


Figure 4. Differential resistance (dv/di) at room temperature for an air-bridge microbolometer in an evacuated environment compared to an ambient air environment. Also shown are two plots of eq. 1 with R_0 fixed by previous measurements and $\beta = 36.5 \text{ V}/(\text{W}\cdot\text{mA})$ and $\beta = 53.7 \text{ V}/(\text{W}\cdot\text{mA})$.

To better understand the contribution of various device features to the conduction, the values of G were derived from measurements of two different devices from within 5 mm of each other on the same wafer: one measured both in air and in vacuum, and the other device with a much larger thermal conduction (i.e., the final XeF_2 Si etch step was not performed). The measured β and derived thermal conduction (G_{meas}) for these configurations are shown in Table 1 along with the expected conduction (G_{calc}) calculated using reasonable estimates of device geometry and table values for material thermal conductivities.

Table 1. Measured and calculated thermal conduction for various structures of the air-bridge and substrate-supported Nb microbolometers.

	β [V/(W·mA)]	G_{meas} [$\mu\text{W}/\text{K}$]	G_{calc} [$\mu\text{W}/\text{K}$]
Air-bridge evacuated	54	4.5	4.1
Air-bridge in air	37	6.6	(not estimated)
Non-air-bridge on 100 nm SiO_2	1.9	125	130

The excellent agreement between the measured and the calculated values of G should be taken with a grain of salt because of the large ($\sim 10\%$) uncertainties in most of the estimated quantities. However, the good agreement is assurance that the thermal system of the microbolometer is well understood.

The value of G for the evacuated air-bridge is of particular interest, especially in looking toward improving

the devices further. The final calculated value of G , $4.1 \mu\text{W}/\text{K}$, comes from $1.9 \mu\text{W}/\text{K}$ for the lattice conduction of the SiO_2 that encapsulates the Nb, and $2.2 \mu\text{W}/\text{K}$ for the Nb itself. The low- G limit for these bolometers given by the Wiedemann-Franz law is $0.6 \mu\text{W}/\text{K}$. It is clear, therefore, that future designs that eliminate the $\sim 350 \text{ nm}$ of SiO_2 that surrounds the device will further reduce G by a factor of two. When fabricated directly on a thick oxide barrier on Si ($G \approx 25 \mu\text{W}/\text{K}$), the measured thermal time constant is $\tau = 400 \text{ ns}$. Scaling up the time constant with decreasing G gives an estimated time constant for the air-bridge of $\tau = 2 \mu\text{s}$, which is still much smaller than the maximum $10 \mu\text{s}$ required for the proposed full-body scanning system.⁶

5. CONCLUSION

We have demonstrated a simple process for producing hundreds of 100 GHz detector pixels on a single wafer with good sensitivity. Although the sensitivity is far below that required for passive imaging, active systems benefit greatly from the reduced system cost and complexity of these devices. The process described is a 4-mask, all-optical-lithography process that uses standard wafer processing equipment and a Bosch-process deep etcher. By eliminating the parasitic SiO_2 on future air-bridge devices we expect to further improve the device sensitivity to $\sim 10 \text{ pW}/\sqrt{\text{Hz}}$. Furthermore, if we can achieve the Wiedemann-Franz thermal conductivity limit for these devices of $G = 0.6 \mu\text{W}/\text{K}$ the device sensitivity improves to $\sim 5 \text{ pW}/\sqrt{\text{Hz}}$. Any improvements to the sensitivity allows higher signal-to-noise imaging for existing 100 GHz sources and significantly simplifies the construction of higher-frequency ($> 500 \text{ GHz}$) imaging tools for long-range moderate-resolution or short-range high-resolution detection of concealed weapons.

ACKNOWLEDGMENTS

The authors thank the NIST Office of Law Enforcement Standards, the National Institute of Justice, and the Transportation Security Administration for funding the work leading to this paper.

REFERENCES

1. E. N. Grossman and A. J. Miller, "Active millimeter-wave imaging for concealed weapons detection," *Proc. SPIE - Int. Soc. Opt. Eng. (USA)* vol.5077, pp. 62-70, 2003.
2. E. N. Grossman, A. K. Bhupathiraju, A. J. Miller, and C. D. Reintsema, "Concealed weapons detection using an uncooled millimeter-wave microbolometer system," *Proc. SPIE - Int. Soc. Opt. Eng. (USA)* vol.4719, pp. 364-369, 2002.
3. S. Nolen, T. E. Harvey, C. D. Reintsema, and E. N. Grossman, "Properties of cavity-backed slot-ring antennas at 95 GHz," *Proc. SPIE - Int. Soc. Opt. Eng. (USA)* vol.4373, pp. 49-57, 2001.
4. E. N. Grossman, S. Nolen, N. G. Paulter, and C. D. Reintsema, "Concealed weapons detection system using uncooled, pulsed, imaging arrays of millimeter-wave bolometers," *Proc. SPIE - Int. Soc. Opt. Eng. (USA)* vol.4373, pp. 7-15, 2001.
5. A. Luukanen, A. J. Miller, and E. N. Grossman, "Active millimeter-wave video rate imaging with a staring 120-element microbolometer array," *Proc. SPIE - Int. Soc. Opt. Eng. (USA)* these proceedings, 2004.
6. E. N. Grossman, A. Luukanen, and A. J. Miller, "Terahertz active direct detection imagers," *Proc. SPIE - Int. Soc. Opt. Eng. (USA)* these proceedings, 2004.